Journal of Alloys and Compounds 815 (2020) 152622

Contents lists available at ScienceDirect

Journal of Alloys and Compounds

journal homepage: http://www.elsevier.com/locate/jalcom

Enhancing upconversion luminescence of highly doped lanthanide nanoparticles through phase transition delay

Dekang Xu [a], Feiyan Xie [a], Lu Yao [b], Yongjin Li [b], Hao Lin [c], Anming Li [d], Shenghong Yang [b], Shengliang Zhong [e, *], Yueli Zhang [b, **]

[a] School of Chemistry and Materials Engineering, Huizhou University, Huizhou, 516007, PR China
[b] School of Materials Science and Engineering, Sun Yat-sen University, Guangzhou, 510275, PR China
[c] School of Physics and Electronic Engineering, Guangzhou University, Guangzhou, 510006, PR China
[d] Guangdong Provincial Key Laboratory of Optical Fiber Sensing and Communications, Department of Optoelectronic Engineering, Jinan University, Guangzhou, 510632, China
[e] Research Center for Ultrafine Powder Materials, College of Chemistry and Chemical Engineering, Jiangxi Normal University, Nanchang, 330022, China

ARTICLE INFO

Article history:
Received 16 February 2019
Received in revised form
23 September 2019
Accepted 8 October 2019
Available online 9 October 2019

Keywords:
Rare earth
Nanocrystals
High doping
Upconversion
Phasetransition-delay

ABSTRACT

Doping of rare earth (RE) ions in a low-phonon-energy host matrix is an effective strategy to enhance the upconversion luminescence (UCL) of lanthanide-doped nanoparticles. However, doping of optically inactive RE ions at high concentrations can cause an undesirable phase transition of the host matrix, with concomitant decrease in luminescence. Herein, we present a phase-transition-delay protocol to effectively preserve the pure orthorhombic phase of a KLu_2F_7:Yb^{3+},Er^{3+} system, even at high RE dopant concentrations. The proposed concept can be realized by incorporating a set of optically inactive RE dopants, i.e., Y^{3+} or Gd^{3+}, with different ionic radii to replace the Lu^{3+} ions in the host matrix to overcome the energy barrier of the phase transition. The nanoparticles were synthesized in a high-boiling solvent or at a high reaction temperature. We observed maximal UCL of Er^{3+} at different Y^{3+} or Gd^{3+} dopant concentrations; the optimal Y^{3+} or Gd^{3+} concentration at which maximal UCL is observed is 10 mol% for samples prepared by a water-based hydrothermal route, while it is 30 mol% for samples prepared by an oleic acid-based hydrothermal route. Further, this optimal concentration could be increased to as much as 50 mol% by adopting a high reaction temperature. The high doping of Y^{3+} or Gd^{3+} can efficiently lead to enhanced upconversion performance of the final materials (as much as 32-fold and 9-fold enhancements in the upconversion intensity and quantum yield, respectively, are achieved). The UCL enhancement is caused by the break-down of the symmetry of lanthanide sites in the crystal lattice induced by Y^{3+} or Gd^{3+}, which enhances the energy transfer probabilities between Yb^{3+} and Er^{3+}. Our findings highlight a convenient route to simultaneously tune the phase transition of the host and upconversion output, and this strategy can be applied to other upconversion host materials.

1. Introduction

Lanthanide-based upconversion nanoparticles (UCNPs) have been widely investigated owing to their unique optical property that allows the generation of high-energy light from low-energy light and expands their application in multi-color imaging [1,2], biological tracking and labeling [3–6], and photocatalysis [7–9]. However, the efficiency of the upconversion luminescence (UCL) of lanthanide-based UCNPs, which ranges only up to ~0.3%, is very low due to their nanometric size and large surface-to-volume ratio. To achieve highly efficient UCL, one common strategy is to choose a low-phonon-energy host (normally fluorides). The hexagonal-phase $NaYF_4$, viz., β-$NaYF_4$, is known to be one of the most efficient host lattices [10]. However, due to the appreciable quenching of the UCL caused by the depletion of the excitation energy at higher lanthanide doping concentrations in such host materials, it is necessary to find a suitable host lattice. Recently, orthorhombic KYb_2F_7:Yb^{3+},Er^{3+} UCNPs were shown to effectively preserve the excitation energy owing to the energy-clustering mechanism of the

* Corresponding author.
** Corresponding author.
E-mail addresses: slzhong@jxnu.edu.cn (S. Zhong), stszyl@mail.sysu.edu.cn (Y. Zhang).

https://doi.org/10.1016/j.jallcom.2019.152622
0925-8388/

intrinsic lanthanide-arranged tetrad-cluster structure [11]. Moreover, we have previously synthesized KLu_2F_7:Yb^{3+},Er^{3+} UCNPs and evaluated its UCL performance by J-O theoretical analysis and energy transfer mechanistic investigations in comparison with those of the well-known β-$NaYF_4$:Yb^{3+},Er^{3+} and β-$NaGdF_4$:Yb^{3+},Er^{3+} [12,13] to find that the orthorhombic KLu_2F_7 UCNPs could also be an excellent host material for UCL.

Doping strategy is a simple yet effective way to tune the phase and size of the UCNPs, and hence the lanthanide luminescence [2,14–23]. However, doping the non-emitting ion at a high concentration would cause severe quenching of the luminescence. For example, upon increasing the Gd^{3+} dopant concentration, the corresponding emission intensity of $NaYF_4$:Gd^{3+},Yb^{3+},Er^{3+} nanocrystals increased first and then decreased gradually [14,24], which is due to the increased content of the hexagonal phase in the material structure and a reduction in the particle size with increasing Gd^{3+} dopant concentration. The situation is similar for $NaYF_4$:Yb^{3+},Er^{3+} nanocrystals doped with Fe^{3+} [25]. The introduction of lanthanide ions would, however, induce a phase transition in fluoride nanocrystals. By doping La^{3+} ions into hexagonal $NaLuF_4$:Yb^{3+},Er^{3+} nanocrystals, a phase transition from hexagonal to cubic structure was achieved, leading to reduced crystallite size and hence UCL [24]. It was found that KYb_2F_7:Yb^{3+},Er^{3+} nanocrystals underwent phase transition upon Gd^{3+} doping (orthorhombic KYb_2F_7 structure to cubic $KGdF_4$ structure), which resulted in a dramatic reduction in the UCL with a further increase in the Gd^{3+} concentration [26]. Recently, the effect of the ionic radii of different metal ions on the size and phase transition of KLu_2F_7 UCNPs was investigated, and the phase transition was found to be mainly caused by size reduction of the particles [27,28]. Therefore, it remains a challenge to control the phase transition of the host when it is doped with a high concentration of lanthanide ions for enhancing the UCL.

In this work, we observed the phase transition of KLu_2F_7:Yb^{3+},Er^{3+} UCNPs incorporated with four kinds of optically inactive RE ions, Y^{3+}, La^{3+}, Y^{3+} and Gd^{3+}, with different ionic radii as compared to that of Lu^{3+}. We successfully realized a phase transition delay (PTD) even at higher doping concentrations of RE ions by adjusting the experimental conditions, such as by adopting a high-boiling solvent (oleic acid, OA) or using a high reaction temperature (up to 260 °C). We found that the samples prepared by different methods show different maximal Er^{3+} UCL intensities at different RE concentrations, owing to the high doping level in a stable orthorhombic KLu_2F_7 phase realized by the PTD effect.

2. Experimental methods

2.1. Materials

Lu_2O_3 (99.99%), Er_2O_3 (99.99%), Yb_2O_3 (99.99%), Y_2O_3 (99.99%), Gd_2O_3 (99.99%), La_2O_3 (99.99%), KF (99%), dipotassium ethylene diamine tetraacetate K_2-EDTA (99%), oleic acid OA (AR), ethanol (AR), and HNO_3 (65%) were purchased from Aladin Corporation and used as received without further purification.

2.2. Preparation of rare-earth nitrate stock solution

An $RE(NO)_3$ (RE = Y, Lu, Yb, Er, Gd, or La) solution was prepared by adding a known amount of RE_2O_3 into a concentrated HNO_3 solution with heating in a water bath until the excess HNO_3 evaporated. Thereafter, an appropriate amount of deionized water was added with agitation to obtain a clear solution with a known concentration. Specifically, the stock solutions of $Y(NO_3)_3$, $Lu(NO_3)_3$, and $Gd(NO_3)_3$ were prepared at 1 mol/L concentration. The $Yb(NO_3)_3$ solution was prepared at 0.5 mol/L, the $La(NO_3)_3$ solution was prepared at 0.25 mol/L, and the $Er(NO_3)_3$ solution was prepared at 0.1 mol/L concentration.

2.3. Synthesis of UCNPs doped with variable amounts of RE ions by a water-based hydrothermal route

A $Ln(NO_3)_3$ solution (1 mmol in total with Ln = (100−x)%Lu, 18% Yb, 2%Er, x%RE, RE = Yb, Y, Gd, La, x = 0, 10, 20, 30, 40, 60, 80, and 100 for Y, Gd, La, and x = 0, 25, 50, 75, and 100 for Yb, respectively) was added to an appropriate amount of deionized water with agitation. Then, 3.75 mL of a K_2-EDTA solution (0.4 M) was added to form a white turbid liquid. A transparent colloid was formed by the subsequent addition of KF (12 mmol), and the mixture was stirred for 30 min. Subsequently, the mixture was transferred into an autoclave and heated at 180 °C for 12 h. The final products were collected by centrifugation, washed with ethanol, and dried overnight at 80 °C.

2.4. Synthesis of UCNPs doped with variable amounts of RE ions by an OA-based hydrothermal route

First, 2 mL of OA, 10 mL of ethanol, and KOH (4 mmol) were mixed together to form a transparent solution and stirred for 10 min. Then, a $Ln(NO_3)_3$ solution (1 mmol in total; Ln = (100−x)% Lu, 18%Yb, 2%Er, x%RE, RE = Yb, Y, Gd, x = 0, 10, 20, 30, 40, 60, 80, and 100 for Y and Gd, and x = 0, 25, 50, 75, and 100 for Yb, respectively) was added to 12 mL of deionized water with agitation. Next, the diluted rare earth nitrate solution was added to the transparent OA solution to form a white turbid liquid and stirred for 10 min. A transparent colloid was formed by the subsequent addition of KF (8 mmol), and the mixture was stirred for 30 min before being sealed in an autoclave and heated at 180 °C for 12 h. The final products were collected by centrifugation, washed with ethanol, and dried overnight at 80 °C.

2.5. Synthesis of UCNPs doped with variable amounts of Y ions by an OA-based hydrothermal route at a higher temperature

First, 2 mL of OA, 10 mL of ethanol, and KOH (4 mmol) were mixed together to form a transparent solution and stirred for 10 min. Then a $Ln(NO_3)_3$ solution (1 mmol in total; Ln = (100-x)%Lu, 18%Yb, 2%Er, x%Y, x = 0, 10, 20, 30, 40, 60, 80, and 100) was added to 12 mL of deionized water with agitation. Then, the diluted rare earth nitrate solution was added to the transparent solution to form a white turbid liquid and stirred for 10 min. A transparent colloid was formed by the subsequent addition of KF (8 mmol), and the mixture was stirred for 30 min before being sealed in an autoclave and heated at 260 °C for 12 h. The final products were collected by centrifugation, washed with ethanol, and dried overnight at 80 °C.

2.6. Characterization of the samples

The structure of the samples was characterized by X-ray diffraction (XRD; Rigaku D-Max 2200 VPC, XRD, Cu *Kα* radiation). The morphologies of the samples were studied using a thermal field scanning electron microscope (FEI Quanta 400FEG, working voltage = 30 kV) and a transmittance electron microscope (FEI Tecnai G2 Spirit, acceleration voltage = 120 kV). UCL spectra were recorded on a combined fluorescence lifetime and steady-state spectrometer (Edinburgh FLS920) equipped with a cw 974-nm laser diode. The lifetime measurements were performed on a photoluminescence spectrometer (Edinburgh FLS980) equipped with a pulsed 980-nm laser diode. The UCL quantum yield (QY) was measured on Ocean Optics QE65Pro integrated with a 974 nm laser.

3. Results & discussion

The KLu_2F_7:Yb^{3+},Er^{3+} UCNPs prepared in this work usually crystallize into an orthorhombic structure (Fig. S1, ESI), which is in agreement with the previous reports on such materials [11,29–31]. We have previously verified that the orthorhombic KLu_2F_7 phase is thermodynamically stable when compared to the cubic KLu_3F_{10} counterpart, and thus shows highly efficient UCL [13]. When doped with lighter and larger RE ions at high concentrations (as compared with the heaviest, small-sized Lu^{3+}) (Table S1, ESI), the lanthanide sites in the KLu_2F_7 crystal undergo a significant electron cloud distortion, which could lead to structural distortion and phase transition [14]. In this work, the doping of RE ions into the KLu_2F_7 host leads to phase transition from the orthorhombic to cubic phase (Fig. 1(a)). To investigate the doping effect, we doped four types of RE ions (Yb^{3+}, Y^{3+}, Gd^{3+}, La^{3+}) into the orthorhombic KLu_2F_7:Yb^{3+},Er^{3+} UCNPs prepared by the water-based hydrothermal route. As shown in Fig. 1(b), the XRD pattern of undoped KLu_2F_7 UCNPs can be indexed well with the orthorhombic KLu_2F_7 phase. It is also found that with the doping of 25 mol% Yb^{3+} and 10 mol% Y^{3+}, the structures of UCNPs remained unchanged, as only slight shifts in the diffraction peaks to lower angles are observed due to the lattice expansion caused by the larger ions doped in the host matrix. Upon doping with larger sized RE ions, 10 mol% Gd^{3+} and 10 mol% La^{3+}, the cubic phase starts to emerge and the XRD peak intensity increases gradually following the introduction of larger ions. We also doped the RE ions at different concentration in the UCNPs (see Fig. 2). Upon doping RE^{3+} ions with different ionic sizes, the critical concentration corresponding to the completion of the orthorhombic-to-cubic phase transformation changes; the critical concentration is 75 mol% for Yb^{3+} doping, 60 mol% for Y^{3+} doping, and 40 mol% for Gd^{3+} doping. As for La^{3+} doping, the phase-transition process is complicated due to the large disparity in the ionic sizes of La^{3+} and Lu^{3+} (Table S2, ESI). When the La^{3+} doping concentration is 30 mol%, three distinct phases exist: orthorhombic KLu_2F_7, cubic K(Lu/La)F_4, and hexagonal LaF_3. A pure LaF_3 phase is formed when the La^{3+} concentration is greater than 80 mol%. Nevertheless, all the diffraction peaks were observed to shift towards lower angles with increasing RE^{3+} ion concentration, which suggested the successful substitution of Lu^{3+} ions by larger RE^{3+} ions.

To elucidate the effect of doping on the phase transition of KLu_2F_7, we performed first-principle calculations based on the density functional theory (DFT) to determine the formation energies of KLu_2F_7 UCNPs and Y^{3+}-doped KLu_2F_7 UCNPs in their orthorhombic and cubic forms (Fig. S2 and Table S3, ESI), respectively. The DFT calculations were executed with the DMol3 module on Materials Studio platform. We chose the local density

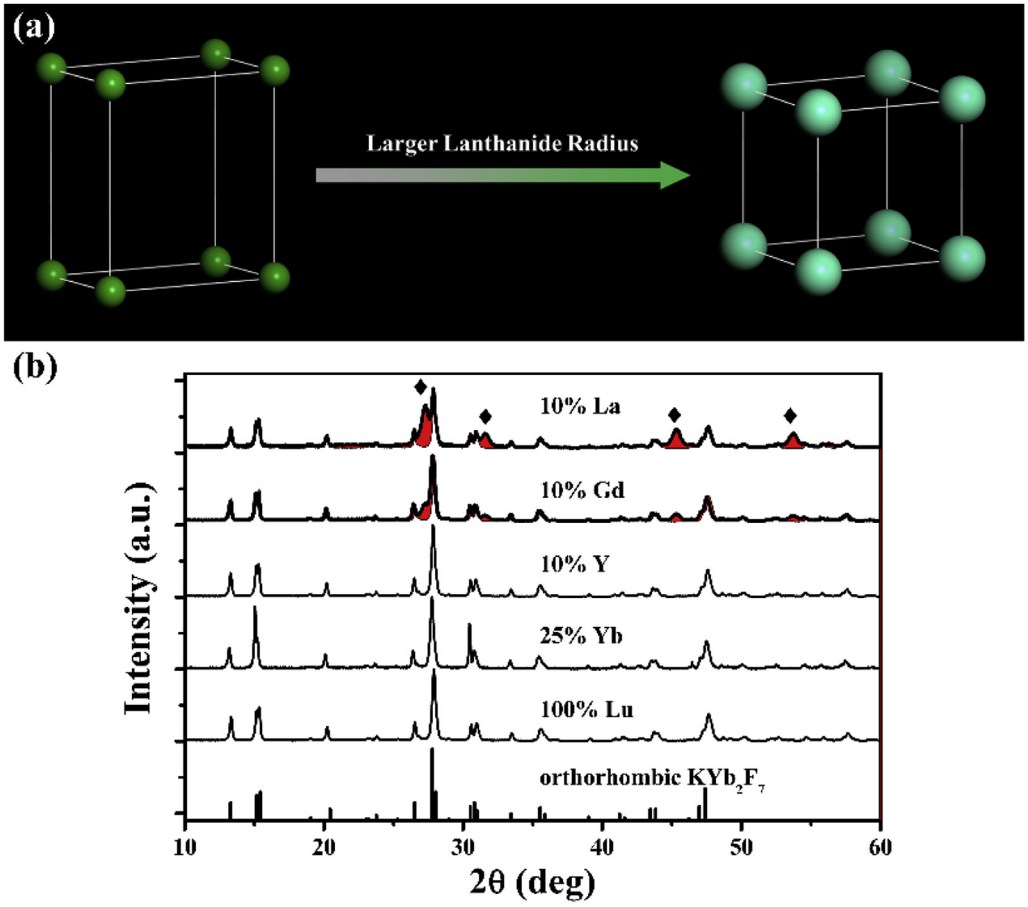

Fig. 1. Lanthanide-doping induced phase transition of KLu_2F_7. (a) General trend of the phase transition from orthorhombic KLu_2F_7 to cubic KRE_xF_{1+3x} with the substitution of Lu^{3+} with RE^{3+} of larger ionic radii. Green spheres represent smaller Lu ions. Cyan spheres represent RE ions with larger ionic radii. (b) XRD patterns of KLu_2F_7:18%Yb^{3+},2%Er^{3+}, $K(Lu_{0.75}Yb_{0.25})_2F_7$:18%$Yb^{3+}$,2%$Er^{3+}$, $K(Lu_{0.9}Gd_{0.1})_2F_7$:18%Yb^{3+},2%Er^{3+}, and $K(Lu_{0.9}La_{0.1})_2F_7$:18%Yb^{3+},2%Er^{3+} UCNPs. The pure KLu_2F_7 structure matches well with that of the orthorhombic KLu_2F_7 phase (space group: $Pna2_1$). The diamond symbol indicates the presence of the cubic KRE_xF_{1+3x} structure (For RE = Yb and Y, $x = 3$; For RE = Gd and La, $x = 1$). A gradual increase in the diffraction peak intensities of the cubic phase is observed as a function of the ionic radius of the RE^{3+} dopant (the red zone). The standard diffraction peaks of KYb_2F_7 could be used as a reference because of the similar ionic radii of Lu^{3+} (0.861 Å) and Yb^{3+} (0.868 Å). (For interpretation of the references to color in this figure legend, the reader is referred to the Web version of this article.)

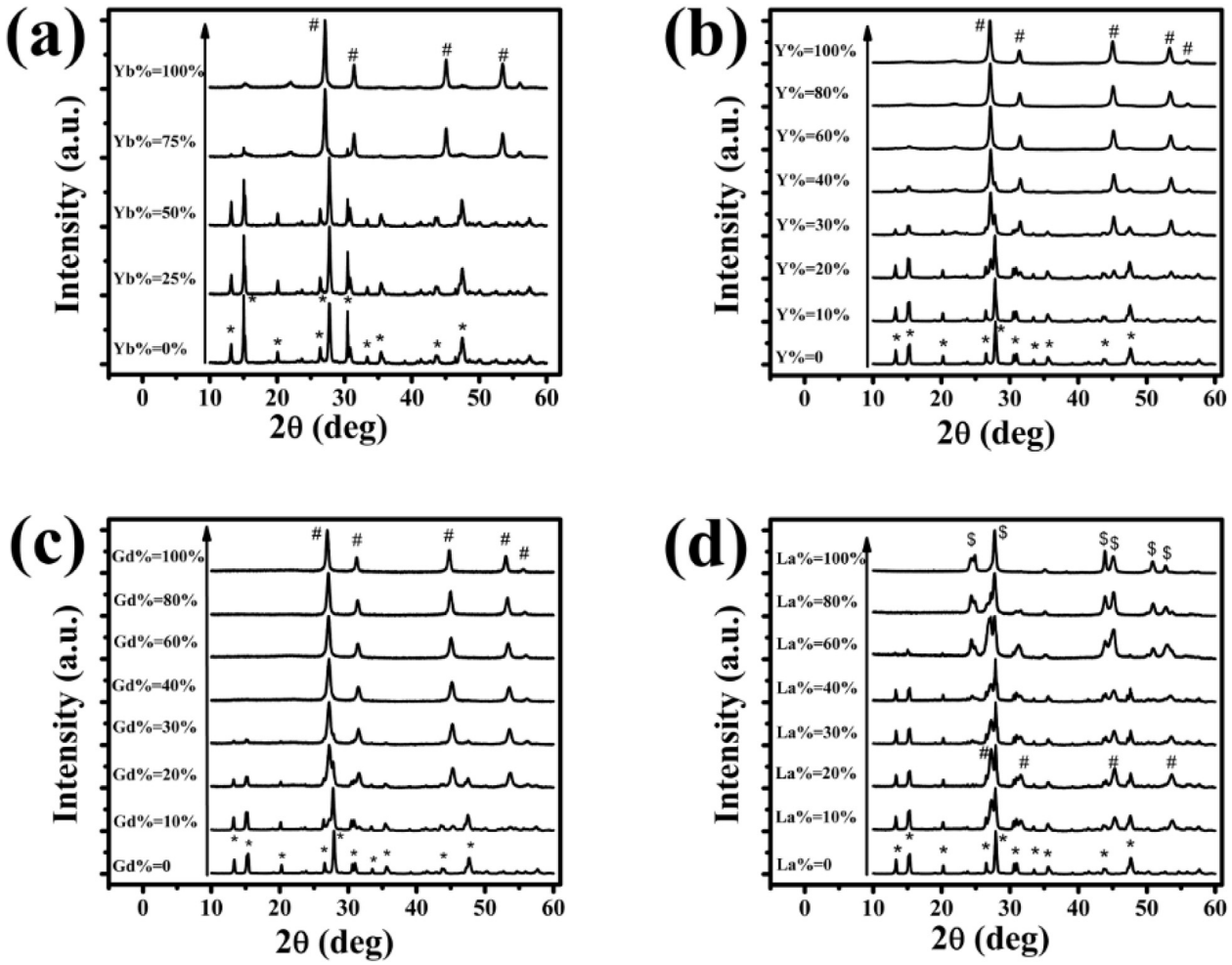

Fig. 2. X-ray diffraction patterns of $K(Lu_{1-m}RE_m)_2F_7$:18%Yb^{3+},2%Er^{3+} nanocrystals doped with various concentrations ($m = 0$–100%) of RE^{3+} (RE = Yb, Y, Gd, and La) ions prepared by the water-based hydrothermal route. "*" symbols stand for the typical orthorhombic structure of KLu_2F_7. "#" symbols stand for the cubic phase. Specifically, cubic KYb_3F_{10} and KY_3F_{10} structure for Yb^{3+} and Y^{3+} doping, and cubic $KGdF_4$ and $KLaF_4$ for Gd^{3+} and La^{3+} doping, respectively. "$" symbols represent the hexagonal LaF_3 phase.

approximation (LDA) with Perdew-Wang LDA function and ultrasoft pseudopotentials to describe the exchange-correlation effects and electron-ion interactions, respectively. The double numerical plus polarization basis set was used to describe the valence orbitals of the atoms. For self-consistent field calculations, the convergence criteria for the total energy was set to $2.0\,E^{-5}$ hartree [32]. The formation energy is defined as the difference between the energies of the unit cell and all isolated atoms, expressed as, $E_{form} = E_{cell} - \sum E_{atom}$. Note that, the more negative the formation energy is (that is, the higher the formation energy is), the more stable the structure. The orthorhombic KY_2F_7 has a lower total energy than KLu_2F_7 owing to its lighter Y element. However, the structure has a higher formation energy, and is thus more stable than that of KLu_2F_7. We also found that the cubic-phase KY_3F_{10} has the largest negative energy, which implies that cubic KY_3F_{10} is the most stable structure. Other cubic forms, such as $KLuF_4$ and KYF_4, have the smallest negative energies, which imply that the cubic forms of these materials are less stable. Therefore, it is reasonable to assume that upon increasing the Y^{3+} concentration, the ionic mismatch would induce the charge density distortion of Lu^{3+} sites, leading to the phase transition from orthorhombic KLu_2F_7 to cubic KY_3F_{10}, and the generation of a more compact structure [14].

Fig. 3 shows the morphologies of KLu_2F_7:18%Yb^{3+},2%Er^{3+} UCNPs with variable amounts of Y^{3+} ions that were obtained by the water-based hydrothermal route. At less than 10 mol% Y^{3+} doping, hexagonal polygonal UCNPs ~200 nm in dimensions are formed (Fig. 3(a)). When doped with 20 mol% Y^{3+}, some small cubic-phase nanocrystals emerge, and the size of the orthorhombic UCNPs is reduced (Fig. 3(b)). When the doping concentration is increased up to 60 mol%, the NPs are completely converted to cubic KY_3F_{10} with spherical particles of ~20 nm in dimensions, as shown in Fig. 3(c) and (d). The structural evolution of Y^{3+}-doped NPs prepared by the water-based route is also obvious from the results presented in Fig. 2(b). This process is illustrated in Fig. 3(e).

One major challenge for realizing the PTD is to overcome the higher formation energy of the cubic structure. We first modified the reaction environment, that is, the raw materials were dispersed in a high-boiling solvent, OA. As oleate salts have been proven to successfully mediate the phase transformation of $NaYF_4$ from the cubic to hexagonal phase [32], it is reasonable to deduce that the oleate salt could favor the formation of orthorhombic KLu_2F_7 at higher RE doping concentrations. Moreover, OA is usually used as a stabilizing agent to control the size and shape of UCNPs [14,33–35]. In this work, KOH was adopted to form the potassium oleate salt, KOA, at the beginning of the reaction, which could effectively induce the formation of the dynamically-stable orthorhombic phase of KLu_2F_7. Fig. 4 shows the morphologies of KLu_2F_7:Yb^{3+},Er^{3+} UCNPs doped with various concentrations of Y^{3+} ions prepared by

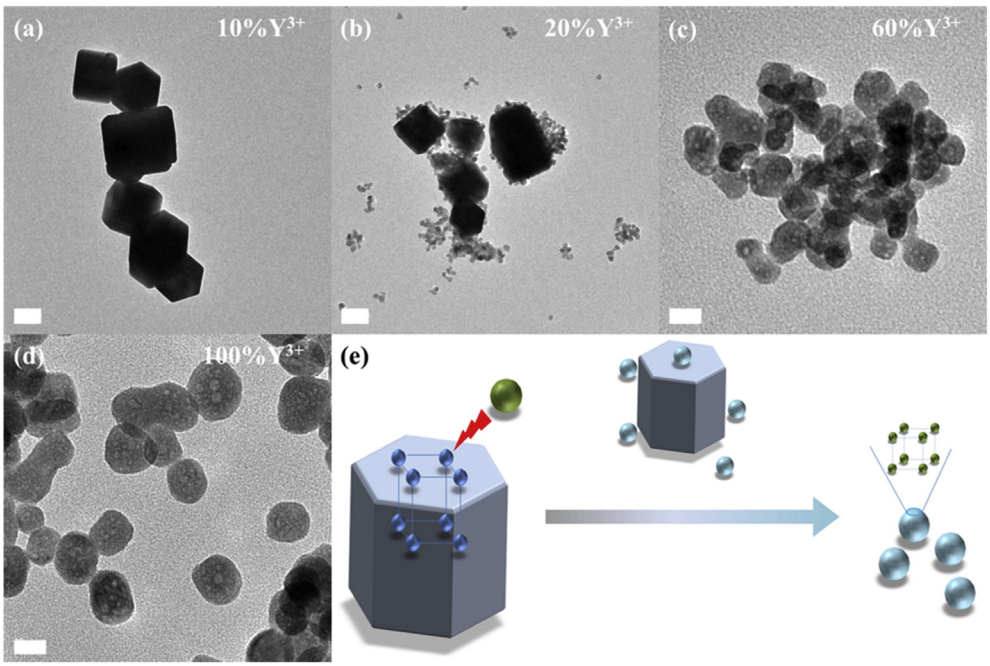

Fig. 3. Morphologies of KLu_2F_7:18%Yb^{3+},2%Er^{3+} UCNPs prepared by the water-based hydrothermal route. (a)–(d) TEM images of KLu_2F_7:xY^{3+},18%Yb^{3+},2%Er^{3+} UCNPs containing various Y^{3+} contents. **(e)** Illustration of the morphological evolution of KLu_2F_7:18%Yb^{3+},2%Er^{3+} UCNPs doped with RE^{3+} of a larger ionic radius. Blue spheres represent smaller Lu ions. Olive green spheres represent larger RE ions. Cubic phase begins to emerge as larger RE ions substitute Lu ions, and the samples present mixed morphologies with hexagonal prism- and sphere-like shape. Scale bar is 100 nm for (a) and (b), and 20 nm for (c) and (d). (For interpretation of the references to color in this figure legend, the reader is referred to the Web version of this article.)

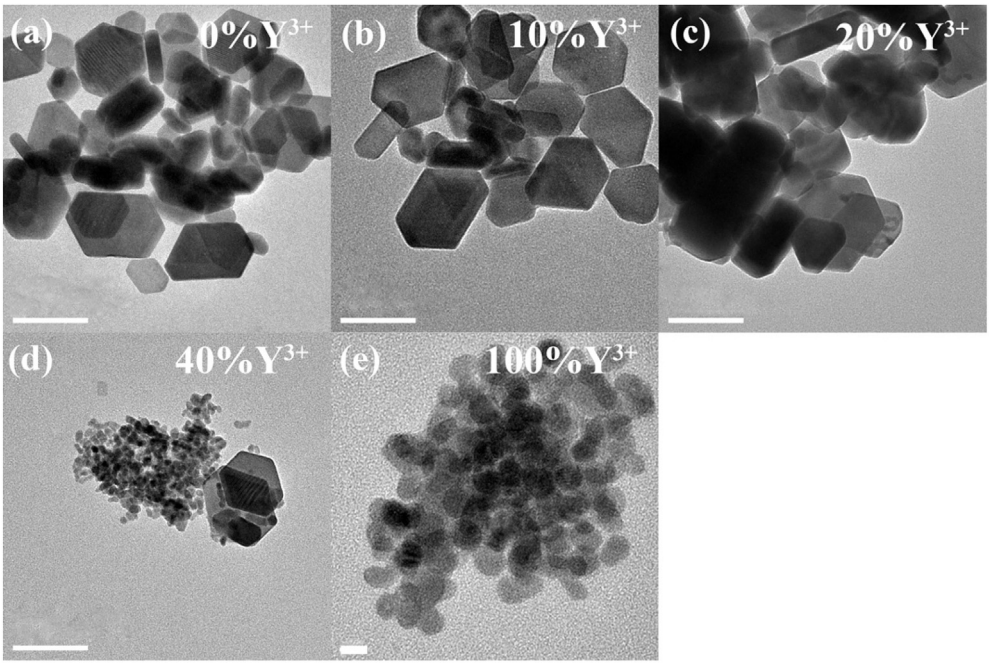

Fig. 4. Morphologies of KLu_2F_7:18%Yb^{3+},2%Er^{3+} UCNPs prepared by the oleic acid-based hydrothermal treatment. (a)–(e) TEM images of KLu_2F_7:xY^{3+},18%Yb^{3+},2%Er^{3+} UCNPs in the presence of containing various Y^{3+} contents. Scale bar is 100 nm for (a)–(d), and 10 nm for (e).

the OA-based hydrothermal route. When Y^{3+} concentration is within 20 mol%, the UCNPs show plate-like shapes with hexagonal cross-section (~100 nm in dimensions). The cubic-phase nanoparticles start to appear at the doping concentration of 30 mol% (Fig. 5(b)), and the ratio of cubic-phase UCNPs increases continuously with increasing doping concentration. The initial phase completely transforms to cubic phase at Y^{3+} concentrations greater than 60 mol%, and the dimension of the nanoparticles is ~10 nm. We also prepared KLu_2F_7:Yb^{3+},Er^{3+} UCNPs doped with different amounts of Yb^{3+} and Gd^{3+} ions (Fig. 5(a) and (c)). It can be obviously observed that with Gd^{3+} doping, the samples are of pure orthorhombic phase until the doping concentration exceeds 10 mol

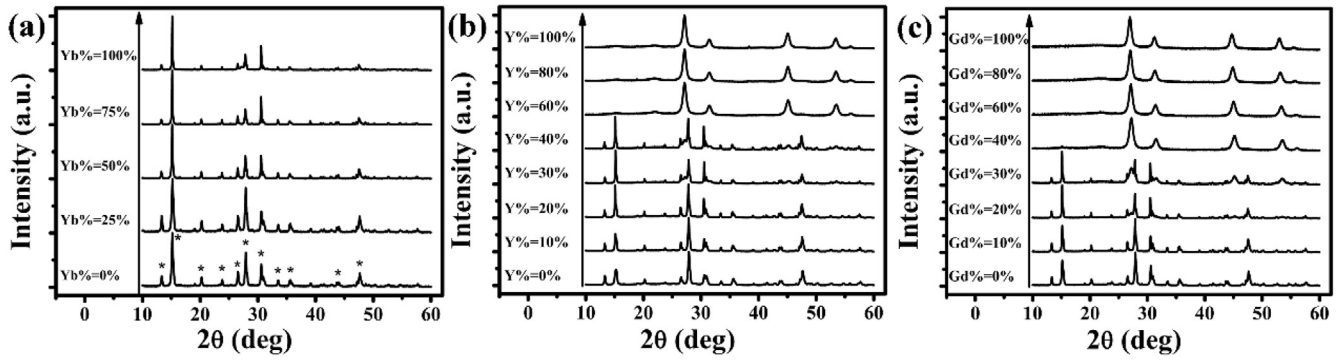

Fig. 5. X-ray diffraction patterns of $K(Lu_{1-m}RE_m)_2F_7$:18%Yb^{3+},2%Er^{3+} nanocrystals doped with various concentrations ($m = 0$–100%) of RE^{3+} (RE = Yb, Y, and Gd) prepared by the OA-based hydrothermal route. Those doped with Yb^{3+} have pure orthorhombic structure. For Y^{3+} doping, the cubic phase starts to form when the Y^{3+} concentration is 30%. The phase-transition concentration is 20% for those doped with Gd^{3+}. The above results suggest a phase-transition-delay phenomenon in a high-boiling solvent environment.

%. The PTD effect is much more distinct when doped with Yb^{3+} ions; in this case, all the samples present pure orthorhombic structures owing to the similar ionic radii of Yb^{3+} and Lu^{3+} (Tables S1 and S2, ESI). The results from UCNPs prepared by the OA-based hydrothermal route compared to those from the UCNPs obtained by the water-based method suggest that the PTD effect is successfully realized not only through smaller ionic size mismatch but also through the variation of the reaction conditions. This is because in OA-based solvent environment, the oleate ions can effectively facilitate the arrangement of Lu^{3+} and lower the energy barrier [32] to maintain the thermodynamically stable phase, the orthorhombic phase. Moreover, the PTD effect of KLu_2F_7 host is much more obvious upon doping RE^{3+} ion with a smaller ionic size mismatch compared to that of the Lu^{3+} ion.

Having successfully observed the PTD effect in several RE ion-doped KLu_2F_7 UCNPs, even when prepared by different solvent-based hydrothermal routes, we further investigated the influence of this effect on the photoluminescence performance of the UCNPs. First, we confirmed that all samples emit visible UCL (Figs. 6 and 7). Two typical emission bands are observed: green emission bands attributed to $^2H_{11/2}/^4S_{3/2} \rightarrow {}^4I_{15/2}$ transitions and red emission band attributed to the $^4F_{9/2} \rightarrow {}^4I_{15/2}$ transition. A violet emission band attributed to $^2H_{9/2} \rightarrow {}^4I_{15/2}$ transition can also be observed; the intensity of this band is however about two orders of magnitude smaller than those of green and red emission bands. Second, all UCNPs doped with different RE^{3+} ions show maximal upconversion intensities. If Y^{3+} and Gd^{3+}-doped samples prepared by the water-based route are considered for example, both type of UCNPs show maximal luminescence intensities at 10 mol% dopant concentration (Fig. 6(b)–(c)), which is consistent with a previous report on the KYb_2F_7:Yb^{3+},Er^{3+} UCNPs doped with various concentrations of Gd^{3+} ions [26]. The difference is that the degree of variation of the UCL intensity of Y^{3+}-doped UCNPs is less obvious than that of Gd^{3+}-doped UCNPs; the UCL of UCNPs with 10 mol% Y^{3+} doping is comparable to that of 20 mol% Y^{3+}-doped counterpart while the UCL of UCNPs with 10 mol% Gd^{3+} is stronger than the rest of the Gd^{3+}-doped counterparts. However, the samples show optimal UCL at 30 mol% dopant concentration when OA is used as the solvent (Fig. 7(b)–(c)). Under such circumstances, the UCL intensity of 30 mol% Y^{3+}-doped UCNPs is much stronger than those of the other Y^{3+}-doped samples, while the UCL intensity of 30 mol% Gd^{3+}-doped UCNPs is comparable with that of 10 mol% and 20 mol% Gd^{3+}-doped counterparts. Nevertheless, the above results strengthen the viewpoint that the PTD effect realized at higher doping levels of RE^{3+} ions can lead to the enhancement of the UCL.

Despite the difference in the solvent-induced PTD effects, the factor that accounts for the maximal UCL intensities observed at different doping concentrations in this work is the RE^{3+} ion-doping effect, which induces PTD and the break-down of the symmetries of the crystal field of the Ln^{3+} sites at the same time. Lowering the symmetry around Ln^{3+} leads to enhanced luminescence intensity because of the increased probability of the electric dipole transitions [36]. To describe the symmetry of UCNPs doped with different RE^{3+} ions, a relative symmetric degree Δ is proposed, which is defined by the ratio between the weighted difference and the sum of the radii of Lu^{3+} and RE^{3+} ions, expressed as,

$$\Delta = \frac{|(1-x)R_{Lu} - xR_{RE}|}{(1-x)R_{Lu} + xR_{RE}}$$

This parameter suggests that the symmetry of Ln^{3+} sites in a crystal lattice cannot always be "broken" by increasing the dopant concentration. There is a critical concentration above which the symmetry will be "repaired." We calculated the relative degree of symmetry of four types of RE^{3+} ions substituting the Lu^{3+} ion to find that the critical concentrations fall in the range of 45–50% (Fig. 8(c)). In the case of UCNPs obtained by the water-based method, Y^{3+}-doped UCNPs present a pure orthorhombic structure when the doping concentration is increased up to 10 mol% and the cubic phase starts to emerge upon a further increase in the Y^{3+} concentration (Fig. 2(b)). The UCL of 10 mol% Y^{3+}-doped UCNPs is much higher than that of the Y^{3+}-free counterpart, but comparable with that of 20 mol% Y^{3+}-doped UCNPs (Y_water in Fig. 8(a)). This is due to two facts: (i) PTD leads to the best UCL performance of the 10 mol% Y^{3+}-doped UCNPs; (ii) cubic phase starts to appear when the doping concentration is 20 mol%. However, a higher doping concentration implies increased distortion of the crystal lattice and thus increased break-down of the symmetries of Ln^{3+} sites, which makes the UCL of 20 mol% Y^{3+}-doped UCNPs comparable to that of 10 mol% Y^{3+}-doped UCNPs. As for Gd^{3+}-doped UCNPs (Gd_water in Fig. 8(a)), a minor amount of the cubic phase starts to appear at 10 mol% doping (Fig. 2(c)). However, owing to the larger ionic mismatch between Gd^{3+} and Lu^{3+}, the increased distortion in KLu_2F_7 lattice leads to more a distorted crystal field around Lu^{3+} sites, resulting in higher UCL compared to that of the Gd^{3+}-free counterparts, despite the presence of cubic-phase nanocrystals as a minor component. Upon a further increase in the Gd^{3+} doping, more cubic-phase nanoparticles appear and the corresponding UCL decreases by a large margin (Fig. 6(c)). In both situations, the UCL decreases dramatically when the doping concentration is greater than 40 mol%, which is ascribed to not only the gradual phase transition of the material to the cubic form but also to the increased degree of symmetry of Ln^{3+} sites in the KLu_2F_7 lattice (Fig. 8(c)). This analysis is applicable to Y^{3+}- and Gd^{3+}-doped UCNPs prepared

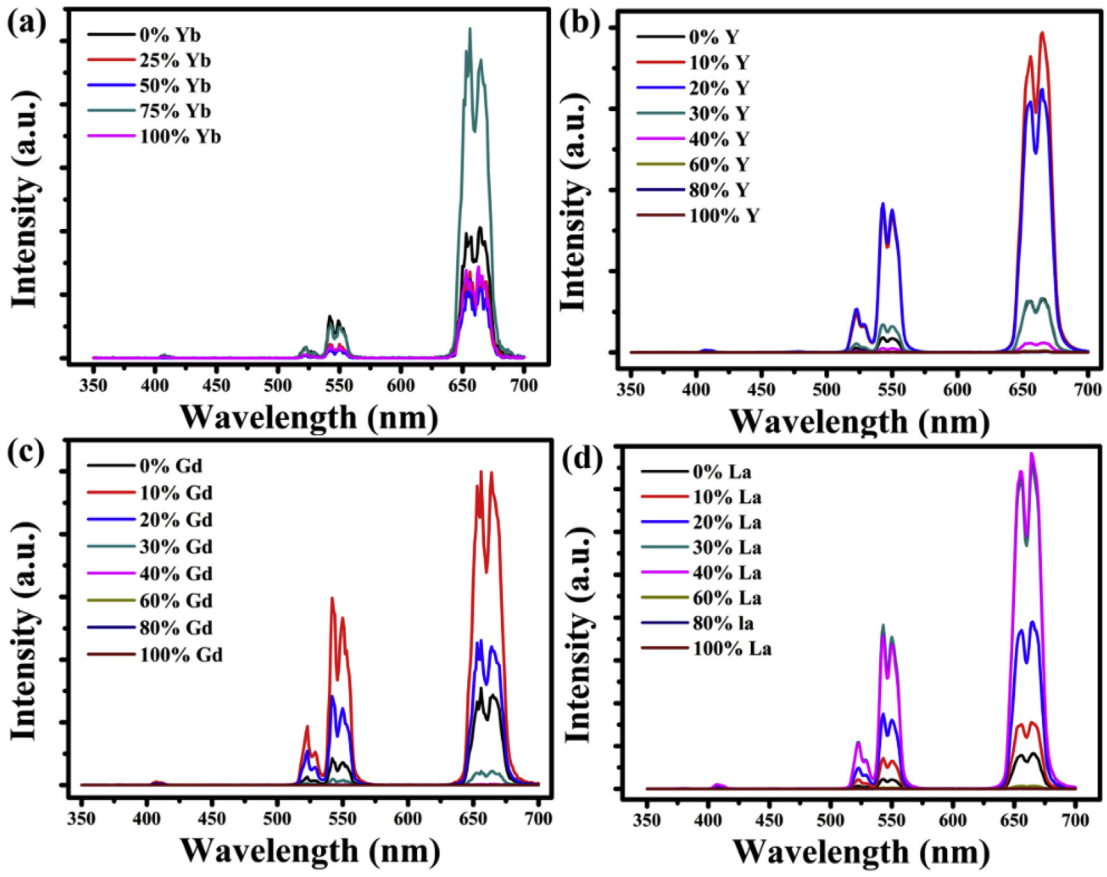

Fig. 6. Upconversion luminescence spectra of $K(Lu_{1-m}RE_m)_2F_7$:18%Yb^{3+},2%Er^{3+} nanocrystals doped with various concentrations ($m = 0$–100%) of RE^{3+} (RE = Yb, Y, Gd, and La) prepared by the water-based hydrothermal route under the excitation of 974 nm cw laser.

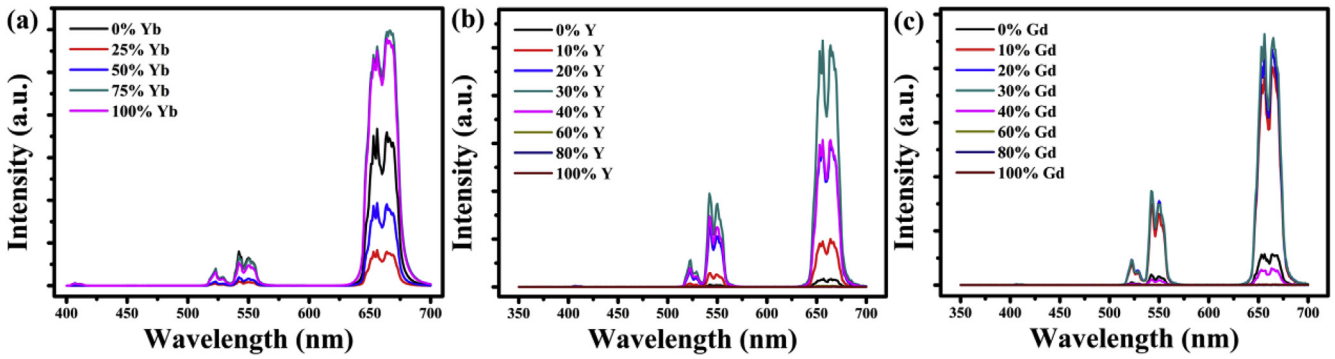

Fig. 7. Upconversion luminescence spectra of $K(Lu_{1-m}RE_m)_2F_7$:18%Yb^{3+},2%Er^{3+} nanocrystals doped with various concentrations ($m = 0$–100%) of RE^{3+} (RE = Yb, Y, and Gd) treated with OA-based hydrothermal route under the excitation of 974 nm cw laser.

by the OA-based method.

In addition, the UCL of RE^{3+} ion-doped UCNPs can be efficiently enhanced by as much as 32 times (Y_OA in Fig. 8(b)) with high doping levels of RE ions. The enhanced UCL of RE^{3+}-doped UCNPs lead to considerably saturated luminescence. The slopes of the emission intensity vs. near-infrared excitation power for both red and green emission are smaller than those of the RE^{3+}-free counterparts (Fig. 8(d) and (e)), which is due to the increasing theoretical lifetimes of the intermediate energy levels of Yb^{3+} and Er^{3+} ions. This can be attributed to the doping effect, which tailors the local crystal field [36] and enables energy transfer upconversion to populate the emissive manifolds. Under such circumstances, the doped UCNPs show a more saturated luminescence [37–40]. Moreover, both green and red emission manifolds possess larger lifetimes for the UCNPs with 30 mol% RE^{3+} doping (Fig. S4, ESI). The increased actual lifetimes are ascribed to the increased theoretical lifetimes of Er^{3+} due to the doping of non-luminous metal ions. The increased theoretical lifetimes of Er^{3+} is caused by the slight change in their corresponding wave functions, which result in more saturated luminescence of the intermediate manifolds [41]. However, with further doping, the corresponding lifetime decreases, which is due to the increasing non-radiative rates caused by the presence of cubic-phase NPs with much smaller sizes that have massive surface quenching sites. To evaluate the effect of PTD on the UCL

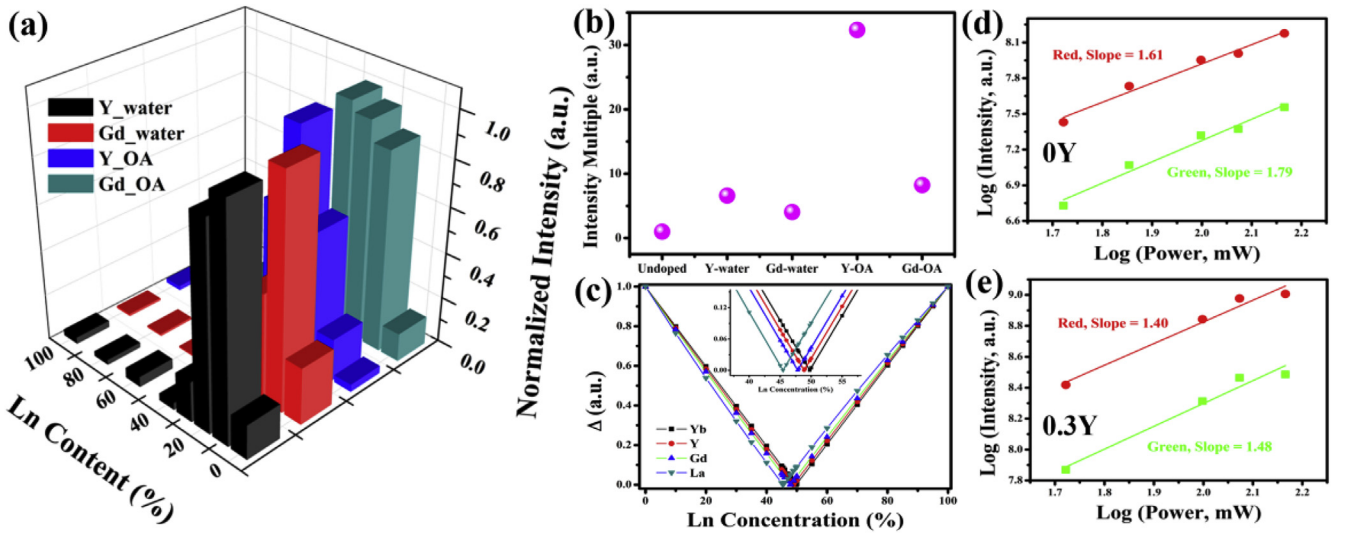

Fig. 8. Upconversion studies of KLu_2F_7:Yb^{3+},Er^{3+} UCNPs doped with various RE^{3+} concentrations; the UCNPS were prepared by water- and oleic acid-based hydrothermal routes. (a) Overall upconversion intensities versus RE^{3+} concentrations. The overall emission intensities are normalized to the maximum intensity. (b) Comparison between the maximum upconversion emission of the undoped and 30 mol% $(Y/Gd)^{3+}$-doped UCNPs. (c) The degree of symmetry Δ of RE^{3+}-to-Lu^{3+} (RE = Yb, Y, Gd, and La) with various concentrations. Inset shows the obvious shifts towards the lower concentration region for RE^{3+} ions with larger ionic radii. (d) and (e) Double logarithmic relationship between the red/green emission intensity and near-infrared excitation power for undoped and 30% Y^{3+}-doped KLu_2F_7:Yb^{3+},Er^{3+} UCNPs prepared by the OA-based method, respectively. (For interpretation of the references to color in this figure legend, the reader is referred to the Web version of this article.)

performance of the UCNPs, we measured the UCL QY of the undoped and 40% Y^{3+}-doped UCNPs. The UCL QY is calculated as follows:

$$QY = \frac{L_{Sa}}{E_{Ref} - E_{Sa}}$$

Here, L_{Sa} is the emission intensity. E_{Ref} and E_{Sa} represent the excited intensities not absorbed by the reference sample and test sample, respectively. The power density of the upconversion excitation is 19.12 W/cm^2. The QYs are calculated to be 0.02% and 0.18% for the undoped and doped UCNPs, respectively, with approximately 9-fold difference. This result confirms the excellent enhancement of the UCL owing to PTD.

We also investigated the effect of the reaction temperature on the PTD behavior of Y^{3+}-doped UCNPs (Figs. 9 and 10). It is clear from Fig. 9 that the UCNPs prepared at high reaction temperature (Fig. 9) remain in the orthorhombic phase even when the doping

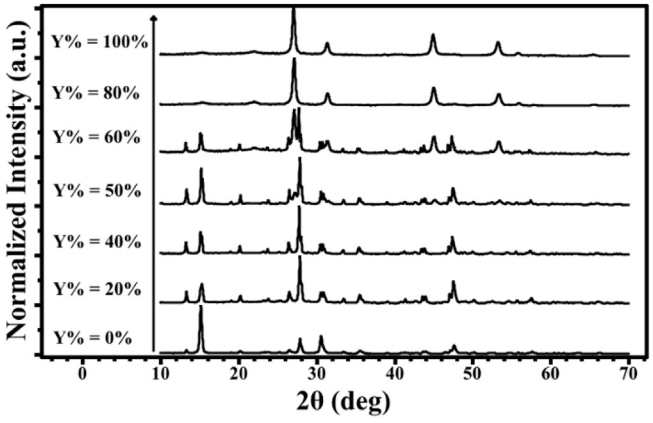

Fig. 9. X-ray diffraction patterns of $K(Lu_{1-m}Y_m)_2F_7$:18%Yb^{3+},2%Er^{3+} nanocrystals at various Y^{3+} concentrations (m = 0–100%); the particles were prepared by the OA-based hydrothermal route at 260 °C. Up to 40 mol% of Y^{3+}, the UCNPs remain in the pure orthorhombic phase.

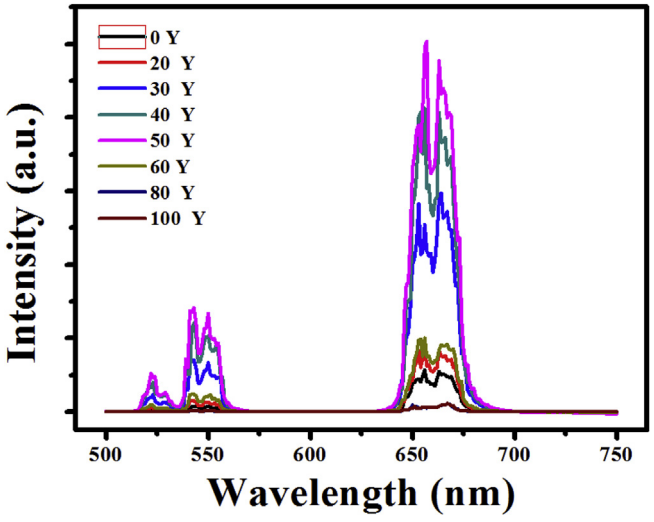

Fig. 10. Upconversion luminescence spectra of $K(Lu_{1-m}Y_m)_2F_7$:18%Yb^{3+},2%Er^{3+} nanocrystals at various Y^{3+} concentrations (m = 0–100%); the particles were prepared by with OA-based hydrothermal route at 260 °C. $K(Lu_{0.5}Y_{0.5})_2F_7$:18%Yb^{3+},2%Er^{3+} nanocrystals show the highest UCL emission.

concentration is 40 mol%. An obvious amount of cubic phase is formed at 50 mol% Y^{3+} doping, and the UCNPs assume the pure cubic phase when the Y^{3+} ion concentration reaches 80 mol%. These structural changes emphasize the remarkable PTD effect. The corresponding UCL spectra (Fig. 10) indicate that 50 mol% Y^{3+} doped UCNPs exhibit the highest UCL. This is also the result of the Y^{3+} doping effect, which tailors the local crystal field and facilitates the formation of a mixed phase.

4. Conclusion

We investigated the PTD effect in the case of KLu_2F_7 UCNPs to prevent the phase transition at high optical inactive RE^{3+} doping levels and thus efficiently enhance their upconversion

performance. The proposed concept presented here can be realized by adopting a set of RE^{3+} dopants with different ionic radii in a high-boiling solvent environment or at a high reaction temperature. Both these methods helped overcome the energy barrier of the phase transition to maintain the pure orthorhombic phase even at high RE^{3+} doping levels. These findings are important not only for understanding the RE^{3+} ion-mediated phase transition process, but also for developing a convenient route to enhance the upconversion performance of lanthanide-doped NPs, which can be extended to other upconversion hosts such as fluorides and oxides.

Acknowledgment

This work was supported by the Program for Innovative Research Team of Huizhou University, National Natural Science Foundation of China (No. 21641008 and 91622105), Jiangxi Provincial Department of Science and Technology (No. 20161BAB203083 and 20172BCB22008), Jiangxi Provincial Education Department (No. GJJ160327), the Scientific Research Foundation of Graduate School of Jiangxi Normal University (No. YC2017-S132), Science and Technology Planning Project of Guangdong Province (Grant No. 2017A010103035), the Natural Science Foundation of Guangdong Province under grant No. 2018030310187, the Fundamental Research Funds for the Central Universities under grant No. 21618310, the Science and Technology project of Huizhou (Grant No. 2016X0421036), the Professorial and Doctoral Scientific Research Foundation of Huizhou University (No. 2018JB012), the Natural Science Foundation of Guangdong Province (No. 2016A030313118), and Department of Education of Guangdong Province (Grant No. 2018KQNCX249).

Appendix A. Supplementary data

Supplementary data to this article can be found online at https://doi.org/10.1016/j.jallcom.2019.152622.

References

[1] S. Heer, K. Kömpe, H.U. Güdel, M. Haase, Adv. Mater. 16 (2004) 2102–2105.
[2] F. Wang, X.G. Liu, J. Am. Chem. Soc. 130 (2008) 5642–5643.
[3] S.F. Lim, R. Riehn, W.S. Ryu, N. Khanarian, C.K. Tung, D. Tank, R.H. Austin, Nano Lett. 6 (2006) 169–174.
[4] L.Q. Xiong, Z.G. Chen, M.X. Yu, F.Y. Li, C. Liu, C.H. Huang, Biomaterials 30 (2009) 5592–5600.
[5] K. König, J. Microsc. 200 (2000) 83–104.
[6] X.F. Yu, L.D. Chen, M. Li, M.Y. Xie, L. Zhou, Y. Li, Q.Q. Wang, Adv. Mater. 20 (2008) 4118–4123.
[7] W.P. Qin, D.S. Zhang, D. Zhao, L.L. Wang, K.Z. Zheng, Chem. Commun. 46 (2010) 2304–2306.
[8] Z.H. Xu, M. Quintanilla, F. Vetrone, A.O. Govorov, M. Chaker, D.L. Ma, Adv. Funct. Mater. 25 (2015) 2950–2960.
[9] J.W. Pickering, V.-R. Bhethanabotla, J.N. Kuhn, Appl. Catal. B Environ. 202 (2017) 147–155.
[10] K.W. Krämer, D. Biner, G. Frei, H.U. Güdel, M.P. Hehlen, S.R. Lüthi, Chem. Mater. 16 (2004) 1244–1251.
[11] J. Wang, R.R. Deng, M.A. Macdonald, B.L. Chen, J.K. Yuan, F. Wang, D.Z. Chi, T.S.A. Hor, P. Zhang, G.K. Liu, X.G. Liu, Nat. Mater. 13 (2014) 157–162.
[12] D.K. Xu, Y. Lu, H. Lin, S.H. Yang, Y. L Zhang, J. Cryst, Growth (2018) 41–45.
[13] D.K. Xu, A.M. Li, L. Yao, H. Lin, S.H. Yang, Y. L Zhang, Sci. Rep. 7 (2017) 43189.
[14] F. Wang, Y. Han, C.S. Lim, Y.H. Lu, J. Wang, J. Xu, H.Y. Chen, C. Zhang, M.H. Hong, X.G. Liu, Nature 463 (2010) 1061–1065.
[15] D.Q. Chen, Y.L. Yu, F. Huang, P. Huang, A.P. Yang, Y.S. Wang, J. Am. Chem. Soc. 132 (2010) 9976–9978.
[16] D.Q. Chen, P. Huang, Y.L. Yu, F. Huang, A.P. Yang, Y.S. Wang, Chem. Commun. 47 (2011) 5801–5803.
[17] H.L. Qiu, G.Y. Chen, R.W. Fan, C. Cheng, S.W. Hao, D.Y. Chen, C.H. Yang, Chem. Commun. 47 (2011) 9648–9650.
[18] Y. Tian, R.N. Hua, B.J. Chen, N.S. Yu, W. Zhang, L.Y. Na, CrystEngComm 14 (2012) 8110–8116.
[19] G. Tian, Z.J. Gu, L.J. Zhou, W.Y. Yin, X.X. Liu, L. Yan, S. Jin, W.L. Ren, G.M. Xing, S.J. Li, Y.L. Zhao, Adv. Mater. 24 (2012) 1226–1231.
[20] H.B. Wang, W. Lu, Z.G. Li, L. Rao, S.J. Zeng, Z. Li, J. Alloy. Comp. 618 (2015) 776–780.
[21] H. Lin, D.K. Xu, D.D. Teng, S.H. Yang, Y.L. Zhang, Luminescence 30 (2015) 723–728.
[22] X.Y. Huang, Opt. Mater. Express 6 (2016) 2165–2176.
[23] X.Y. Huang, B. Li, H. Guo, D.Q. Chen, Dyes Pigments 143 (2017) 86–94.
[24] Y.Q. Wu, Y. Ji, J. Xu, J.J. Liu, Z.W. Lin, Y.L. Zhao, Y. Sun, L. Xu, K.J. Chen, Acta Mater. 131 (2017) 373–379.
[25] J. Tang, L. Chen, J. Li, Z. Wang, J.H. Zhang, L.G. Zhang, Y.S. Luo, X.J. Wang, Nanoscale 7 (2015) 14752–14759.
[26] G.T. Xiang, J.H. Zhang, Z.D. Hao, X. Zhang, Y.S. Luo, S.Z. Lv, H.F. Zhao, CrystEngComm 16 (2014) 249–2507.
[27] X. Xu, Z. Wang, P.P. Lei, X.L. Liu, Y. Su, L.L. Dong, S. Yao, L. Zhou, S.Y. Song, J. Feng, H.J. Zhang, Dalton Trans. 44 (2015) 17286–17292.
[28] X. Xu, X.S. Zhai, K.M. Du, P.P. Lei, L.L. Dong, R.P. Deng, J. Feng, H.J. Zhang, J. Mater. Chem. C 5 (2017) 6311–6318.
[29] Y.C. Li, L.W. Yang, S.X. Yu, Y. Li, P. Wang, X.L. Wei, J.X. Zhong, Ceram. Int. 39 (2013) 7415–7424.
[30] Y.L. Wei, X.M. Li, H. Guo, Opt. Mater. Express 4 (2014) 1367–1372.
[31] Y.L. Wei, H.M. Yang, X.M. Li, L.J. Wang, H. Guo, J. Am. Ceram. Soc. 97 (2014) 2012–2015.
[32] Y.Q. Sui, K. Tao, Q. Tian, K. Sun, J. Phys. Chem. C 116 (2012) 1732–1739.
[33] X. Wang, J. Zhuang, Q. Peng, Y.D. Li, Nature 437 (2005) 121–124.
[34] Z.Q. Li, Y. Zhang, S. Jiang, Adv. Mater. 20 (2008) 4765–4769.
[35] N.J.J. Johnson, W. Oakden, G.J. Stanisz, R.S. Prosser, F.C.J.M. van Veggel, Chem. Mater. 23 (2011) 3714–3722.
[36] S.Y. Han, R.R. Deng, X.J. Xie, X.G. Liu, Angew. Chem. Int. Ed. 53 (2014) 11702–11715.
[37] M. Pollnau, D.R. Gamelin, S.R. Lüthi, H.U. Güdel, Phys. Rev. B 61 (2000) 3337–3346.
[38] G.Y. Chen, G. Somesfalean, Y. Liu, Z.G. Zhang, Q. Sun, F.P. Wang, Phys. Rev. B 75 (2007) 195204.
[39] D.K. Xu, C.F. Liu, J.W. Yan, S.H. Yang, Y.L. Zhang, J. Phys. Chem. C 119 (2015) 6852–6860.
[40] D.K. Xu, H. Lin, A.M. Li, S.H. Yang, Y.L. Zhang, J. Mater. Chem. C 3 (2015) 9869–9876.
[41] G.Y. Chen, H.C. Liu, H.J. Liang, G. Somesfalean, Z.G. Zhang, J. Phys. Chem. C 112 (2008) 12030–12036.